CCFE
CULHAM CENTRE FOR FUSION ENERGY

UK Atomic Energy Authority

UKAEA-CCFE-PR(18)5

A. V. Lunev, S. V. Starikov and V. I. Tseplyaev

Understanding thermally-activated glide of 1/2{110} screw dislocations in UO2 – a molecular dynamics analysis

Understanding thermally-activated glide of 1/2{110} screw dislocations in UO2 – a molecular dynamics analysis

A. V. Lunev,[a, b] S. V. Starikov[a, c] and V. I. Tseplyaev[a, c]

[a]*Joint Institute for High Temperatures of the Russian Academy of Sciences, 13 bld. 2, Izhorskaya st., 125412, Moscow, Russia*
[b]*United Kingdom Atomic Energy Authority (UKAEA), Culham Science Centre, Abingdon, Oxfordshire OX14 3DB, United Kingdom*
[c]*Moscow Institute of Physics and Technology (State University), Dolgoprudny 141700, Moscow, Russia*

This is a preprint of a paper submitted for publication in International Journal of Plasticity

Understanding thermally-activated glide of $1/2\langle 1\,1\,0\rangle\{1\,1\,0\}$ screw dislocations in UO_2 – a molecular dynamics analysis

A. V. Lunev[a,b,*], S. V. Starikov[a,c], V. I. Tseplyaev[a,c]

[a] *Joint Institute for High Temperatures of the Russian Academy of Sciences, 13 bld. 2, Izhorskaya st., 125412, Moscow, Russia*
[b] *United Kingdom Atomic Energy Authority (UKAEA), Culham Science Centre, Abingdon, Oxfordshire OX14 3DB, United Kingdom*
[c] *Moscow Institute of Physics and Technology (State University), Dolgoprudny 141700, Moscow, Russia*

Abstract

As shown experimentally, the interplay between screw and edge dislocations in uranium dioxide (UO_2) determines the low-temperature plasticity in this material. For the latter, neither the mobility of screw dislocations nor the mechanisms of their glide had been assessed – up until now. It is particularly interesting to evaluate the mobility of $1/2\langle 1\,1\,0\rangle\{1\,1\,0\}$ screw dislocations, supposedly the least mobile in UO_2 due to the extremely high Peierls barrier of their motion. To address this issue, molecular dynamics simulations of dislocation glide are conducted on Lomonosov/MVS-10P supercomputers with LAMMPS software, and post-processing is done using DXA/OVITO. Under changing temperature and stress, the following variations of thermally-activated glide are found: nucleation and expansion of double kinks, formation and recombination of $1/6\langle 1\,1\,2\rangle$ Shockley partials, self-pinning and production of debris, formation of sessile $1/3\langle 1\,1\,1\rangle$ Frank loops. Velocity function of $1/2\langle 1\,1\,0\rangle\{1\,1\,0\}$ dislocations calculated at temperaturesu $T = 500$–2000 K and shear stresses $\sigma = 10$–1000 MPa shows a weak temperature dependence and becomes higher than the velocity of $1/2\langle 1\,1\,0\rangle\{0\,0\,1\}$ edge dislocations at temperatures $T < 1250$ K.

*Corresponding author
Email address: artem.lunev@ukaea.uk (A. V. Lunev)

Keywords: A. dislocations; B. ceramic material; C. numerical algorithms; C. atomistic simulation

1. Introduction

There currently exists a certain degree of controversy over the plastic behavior of uranium dioxide. In many papers, polycrystalline (sintered) near-stoichiometric uranium dioxide (UO_2) is reported to have a brittle-to-ductile transition temperature T_{BDT} ranging from approximately 1500 to 1900 K (Scott et al., 1959; Canon et al., 1971; Evans and Davidge, 1969). On the other hand, it was shown in compression experiments of UO_2 single crystals that considerable plastic deformation up to a shear strain $\varepsilon \approx 1\%$ can be achieved for compressive stresses $\sigma = 60$–120 MPa and test temperatures $T = 523$–873 K (Keller et al., 1988b). The typical strain rates in these experiments were $\dot{\varepsilon} = 1 \times 10^{-6}$ – 5×10^{-4} s^{-1}, which implies that low-temperature plastic deformation in UO_2 occurs slowly. These conditions are common to several technological processes, e.g. hot pressing. Therefore, knowledge of low-temperature plasticity might provide ways of improving the fabrication procedure of oxide fuel pellets. In a related case study where $UO_{2.06}$ powder was subjected to hot pressing (temperatures $T = 673$–873 K, axial compaction stress $\sigma \leq 95$ MPa, compaction time $t = 10$–60 min) several evidences of plastic deformation were found by X-ray diffraction: a gradual increase in dislocation density calculated using the Warren-Averbach technique; and texture evolution with compression time manifesting in the displacement of peak pole density on inverse pole figures (IPF) towards $\{0\,0\,1\}$ symmetrically to the $\langle 1\,1\,0\rangle$ directions (Lunev et al., 2017b).

A study by Keller et al. (1988b) reported mostly $1/2\langle 1\,1\,0\rangle\{1\,1\,1\}$ slip traces of screw dislocations after deformation of pre-strained uranium dioxide at temperatures $T = 523$–873 K. Hence, they suggested that the primary slip system at low temperatures in UO_2 is $\langle 1\,1\,0\rangle\{1\,1\,1\}$ – in contrast to the case of high temperatures, at which the primary slip system was found to be $\langle 1\,1\,0\rangle\{0\,0\,1\}$ (Keller et al., 1988a). Other authors are less conclusive on the low-temperature de-

formation in UO_{2+x}. For instance, Alamo et al. (1978) considered the role of $\{1\,1\,1\}$ slip planes only as auxiliary at temperatures $T = 973$–1673 K. Yust and McHargue (1969) pointed out that slip at $T > 1073$ K on $\langle 1\,1\,0\rangle\{1\,1\,0\}$ is also possible. Since little is known from experiments on this topic, one has to rely on simulation data.

According to atomistic modeling, slip of edge dislocation on $\langle 1\,1\,0\rangle\{0\,0\,1\}$ corresponds to the lowest Peierls barrier (Skelton and Walker, 2017; Parfitt et al., 2010; Fossati et al., 2013), while the $1/2\langle 1\,1\,0\rangle\{1\,1\,0\}$ screw dislocations exhibit the lowest line energies Murphy et al. (2014). A recent study by Skelton and Walker (2017) showed that for different interatomic potentials, the $\langle 1\,1\,0\rangle\{1\,1\,0\}$ edge and screw dislocations are characterized by the highest Peierls stresses. Motion of dislocations over the Peierls barrier is thermally activated and usually proceeds by ejection and expansions of double kinks (Kazantsev and Pokrovskii, 1970). Interestingly, there is no direct relation between the value of Peierls stress, which determines the motion of a perfectly straight dislocation at $T = 0$ K, and the characteristics of kinks observed at high temperatures, such as size, shape, and width. It was recently discovered that for edge dislocation in UO_2 at high temperatures, there is a variation in thermally-activated regimes of motion depending on stress and temperature (Lunev et al., 2017a). The motion of dislocation lines can be extremely complex, and standard analytical models might fail to describe the dependence of dislocation velocity on stress and temperature. Returning to screw dislocations in UO_2, their motion has not been studied yet, and it could be that the high Peierls barriers have nothing to do with the real mobility values.

Therefore, this study serves two main purposes: to check whether the supposedly least mobile $1/2\langle 1\,1\,0\rangle\{1\,1\,0\}$ screw dislocations are indeed as slow compared to the edge dislocations on the primary slip system in UO_2; and to extract the temperature and stress dependence of their glide velocity, which may be helpful to the development of a dislocation dynamics code.

2. Methodology

We used LAMMPS simulation package (Plimpton, 1995) which implements the basic molecular dynamics algorithms optimized for machines supporting message-passing interface (MPI). Dump files generated by LAMMPS were subsequently processed with OVITO software (Stukowski, 2010). The latter used the dislocation extraction algorithm (DXA) developed by Stukowski et al. (2012) to visualize dislocation lines and determine their Burgers vectors. Details of the simulation procedure are given below.

2.1. Interatomic potential

It was shown in a recent paper (Lunev et al., 2017a) that MOX-07 (Potashnikov et al., 2011) and Morelon (Morelon et al., 2003) potentials are probably the best available semi-empirical potentials for performing simulation of dislocation motion. Because they are designed based on a relatively simple ionic model, these potentials have strong limitations. They do not allow charge variation of individual ions near the dislocation core, which could be modelled by many-body variable charge potentials – e.g. SMTB-Q or COMB (Sattonnay and Tétot, 2013; Li et al., 2013). However, these latter potentials are still in development. Currently, bulk properties of UO_2 (e.g., lattice parameter, which determines the spacing between adjacent Peierls valleys) are better reproduced using the MOX-07 potential. Another limitation is the impossibility to reproduce Cauchy inequality for UO_2 ($C_{12} \neq C_{44}$) using pair potentials. Interestingly, it was shown (Lunev et al., 2017a; Murphy et al., 2014; Skelton and Walker, 2017) that a many-body EAM potential specifically designed to reproduce elastic constants of UO_2, but otherwise fully based on Yakub pair potential (Yakub et al., 2009), gives virtually identical results for the core structure, line energies, and glide velocity in UO_2. On the other hand, MOX-07 potential also shows good results on surface properties while closely reproducing Pauling empirical relation for electronegativities. The latter is a strong advantage because Coulombic interaction was found to be one of the major factors influencing dislocation mobility. Previous tests showed that MOX-07 and Morelon (Morelon

et al., 2003) potentials displayed very good agreement on the stress dependence of glide velocity of edge dislocations at $T = 2000$ K (Lunev et al., 2017a), and on the line energies and core structures of edge and screw dislocations (Murphy et al., 2014). Morelon potential was recently used by Chartier et al. (2016) to study nucleation of dislocations in UO_2 due to radiation damage and is considered trustworthy. For consistency with previous work, the mobility of screw dislocations was studied with the MOX-07 potential.

2.2. Simulation setup

To simulate dislocation motion, we used the same basic simulation parameters as previously (Lunev et al., 2017a) with a few notable exceptions. Instead of making an orthogonal simulation cell, we introduced a triclinic one characterized by the dimensions L_x, L_y, and L_z and tilt factors xy, xz, yz (Fig. 1). The dislocation line was placed parallel to the x axis in the center of the simulation cell, while glide occurred parallel to the z axis under the applied shear stress σ_{yx}. Periodic boundary conditions were imposed on both x and z axes, while atoms on the boundary xz planes parallel to the y axis had a zero v_y component of their velocities, thus keeping the y–boundaries fixed. Uranium and oxygen atoms were placed in the nodes of a perfect fluorite crystal structure with a non-relaxed lattice parameter $a_0 = 0.54695$ nm. Atoms were then displaced from equilibrium positions according to the expression for the displacement field u of a single screw dislocation derived in classical theory of elasticity (Hirth and Lothe, 1982): $u_x = b/(2\pi) \cdot \mathrm{atan}(y - y_0)/z$, $u_y = 0$, $u_z = 0$, where u_i is the i-th component of the displacement vector, y_0 is the y coordinate of the dislocation core introduced to compensate dislocation drift during system relaxation. A conjugate gradients minimization routine was run each time after the displacement field had been applied. Subsequent relaxation of the simulation cell was done in NVT ensemble with additional minimization of σ_{xx}, σ_{yy}, σ_{zz}, and σ_{xz} stress components introduced via iterative scaling of the L_x, L_y, L_z, and xz dimensions correspondingly.

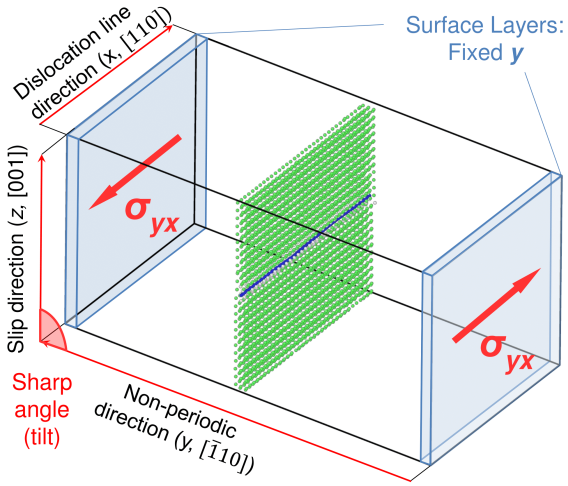

Figure 1: Simulation setup for studying glide of the $1/2[1\,1\,0](1\,1\,0)$ screw dislocation, showing the triclinic simulation cell after relaxation with a finite xz tilt and other dimensions adjusted to minimize normal and shear stresses. Periodic boundary conditions on x and z axes apply, while fixed boundaries are set for the y axis. Atoms in the buffer layers are not allowed to move in the y direction. The dislocation is moved in the z direction by applying shear stress σ_{yx}

3. Results and discussion

Simulation of dislocation glide was performed at temperatures $T = 500$–2000 K (step $\Delta T = 250$ K) and in the range of shear stresses $\sigma = 10$–1000 MPa. The following range of simulation times could be achieved with the available computing power: $t = 0.5$–2.0 ns. Longer runs were required at low stresses and temperatures when the dislocation moved in discrete steps, the time interval between them becoming comparable to the total duration of simulation.

3.1. Preliminary tests

First part of this work consisted in finding the conditions at which converging values for the dislocation glide velocity $v(\sigma, T)$ could be obtained. Hence, further analysis relates to finding whether results depend on the values of L_x (length of the dislocation line), L_y (distance between fixed boundary surfaces), and L_z (length of glide path). All tests were done at a temperature $T = 2000$ K, which is the highest considered in this work. The following dimensions of the

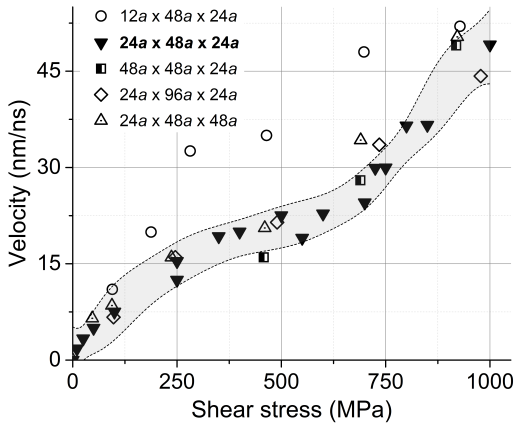

Figure 2: The influence of simulation cell dimensions on the glide velocity of $1/2\langle 1\,1\,0\rangle\{1\,1\,0\}$ screw dislocation in UO_2 at $T = 2000$ K. For sufficiently large simulation cells, the simulation data is confined to a narrow region of the plot (marked in gray), which suggests that converging results are obtained

simulation cells were considered: $12a\times48a\times24a$, $24a\times48a\times24a$, $48a\times48a\times24a$, $24a \times 96a \times 24a$, and $24a \times 48a \times 48a$ where $a(T)$ is the equilibrium crystal structure parameter of UO_2.

Test results (Fig. 2) show that very small dislocation lines ($l = L_x = 12a$) introduce significant error resulting in overestimation of dislocation velocity $v(\sigma)$ at $T = 2000$ K. As discussed by Gilbert et al. (2011), this is mainly because smooth dislocation motion via propagation of kinks on the glide plane is easier when the formation of cross-kinks on orthogonal planes is suppressed. Gilbert et al. (2011) suggested that using shorter dislocation lines, which allow for the formation only of a single kink pair, is preferable. However, because one of the intermediate goals in this work was to establish the modes of thermally activated motion, we considered relatively large values of the L_x dimension. It was expected that the motion of individual kink pairs does not change when increasing simulation box dimensions. As seen on Fig. 2, for sufficiently large simulation cells dislocation velocity is size-independent.

For all configurations considered here, drift of the dislocation line towards y boundaries was noticed. This limits the time of simulation runs. Longer dislocations (higher l) experience stronger non-planar motion at higher stresses. Note that this parasitic drift appears despite the fact that all components of the stress tensor are equilibrated at zero level and the relaxed position of the dislocation line coincided with the center of simulation cell. However, after simulation starts, the σ_{xz} components slowly starts drifting away from zero. It was found that the maximum parasitic σ_{xz} stress depended on the dimensions of the simulation box (e.g., $\sigma_{xz} \leq 20 - 30$ MPa for cells with $L_x = 24a$, $L_y = 96a$ and $L_z = 24a$, $\sigma_{xz} \leq 15 - 20$ MPa for cells with $L_x = 24a$, $L_y = 48a$ and $L_z = 48a$, $\sigma_{xz} \leq 120$ MPa for $L_x = 24a$, $L_y = 48a$ and $L_z = 24a$). However, no correlation was found between the actual value of the parasitic shear stress component σ_{xz} and the glide velocity v_z, as clearly seen from Fig. 2.

The following dimensions of the simulation cell were selected for dislocation velocity calculation: $24a \times 48a \times 24a$ ($330,480$ atoms). For a detailed analysis at high stresses, large simulation cells ($48a \times 48a \times 24a$) were used because of strong bending of dislocations lines.

3.2. Identifying modes of dislocation motion

Specific motion mechanisms of the $1/2\langle 1\,1\,0\rangle\{1\,1\,0\}$ screw dislocation were analyzed based on the shape of the dislocation line evaluated for each stored spatial configurations of atoms discretely registered at equal time intervals for each simulation run. Four distinct modes of dislocation motion (Fig. 3) were distinguished, each of them being activated at different conditions. Below these are presented in order of increasing stress and temperature:

- *Nucleation and expansion of double kinks* (Fig. 3a). Screw dislocations move by ejecting double kinks to the next Peierls valley in their glide direction. If the kink pair is stable, the double kink can then expand, thus resulting in an overall movement of the dislocation on the glide plane. The nucleation rate of critical-sized double kinks, being the limiting factor for

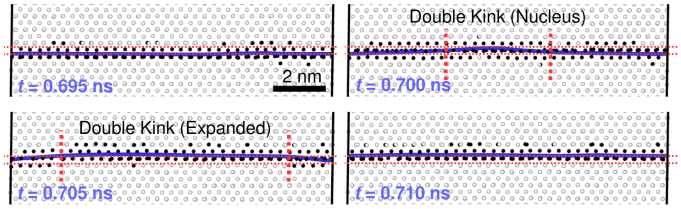

(a)

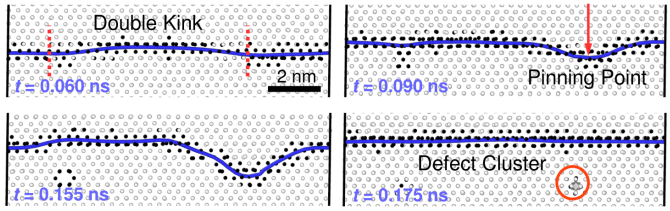

(b)

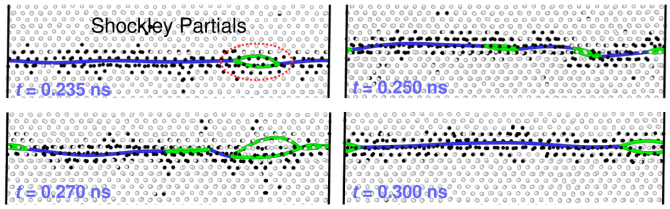

(c)

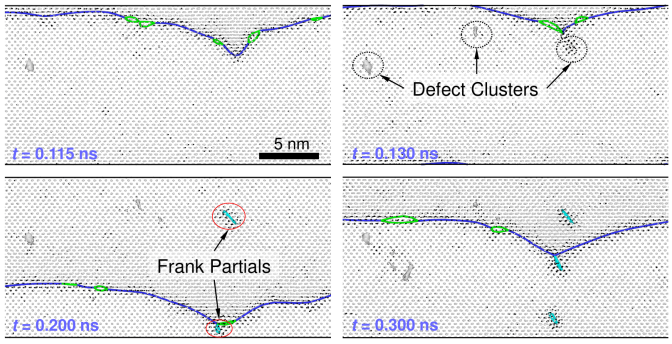

(d)

Figure 3: The different modes of thermally activated motion of the $1/2[1\,1\,0](1\,1\,0)$ screw dislocation in UO_2 as observed in simulations at the following characteristic conditions: (a) $T = 1000$ K, $\sigma = 600$ MPa; (b) $T = 1000$ K, $\sigma = 1000$ MPa; (c) $T = 2000$ K, $\sigma = 100$ MPa; (d) $T = 2000$ K, $\sigma = 1000$ MPa.

this mode of dislocation motion, decreases with temperature and shear stress, meaning an increase in the overall dislocation velocity.

- *Self-pinning and production of defect clusters* (Fig. 3b). At high stresses, self-pinning of the screw dislocation at random points becomes the limiting factor for its motion. This process was first observed in atomistic simulations by Marian et al. (2004). While one of the dislocation segments gets pinned, other can travel relatively far (up to several Peierls valleys from the pinned segment). This results in effectively increasing the dislocation line tension forces, which drag the segment in the glide direction. After unpinning, formation of point defect clusters is often observed. The latter play an additional role in slowing down the screw dislocation, which still moves due to the formation and expansion of double kinks. In this case, however, the limiting process is not the nucleation of double kinks, but the unpinning of individual segments. The latter does not require splitting the perfect dislocation into partials on adjacent atomic planes. Interestingly, the pinning-unpinning motion is somewhat similar to the high-temperature 'vibrating string' mode for $1/2\langle 1\,1\,0\rangle\{0\,0\,1\}$ edge dislocation (Lunev et al., 2017a). The difference is that in case of edge dislocations, their motion resembles a loose string being gently pulled in the glide direction (and thus experiencing large bending), while for screw dislocations the apparent resistance to moving it seems higher and results in high tension forces.

- *Partial splitting* (Fig. 3c). Individual segments of the dislocation line experience occasional splitting into $1/6\langle 1\,1\,2\rangle$ Shockley partials, while the dislocation line as a whole still resembles some degree of integrity. This splitting is very unstable, and the effective loops formed by Shockley partials enclosing intrinsic stacking faults on the $\{1\,1\,1\}$ planes experience rapid constriction. This originates from the very high corresponding stacking fault energy (0.96 J/m^2 as reported by Fossati et al. (2013)). However, the nucleation rate of this splitting increases with temperature and shear

stress. The configuration on Fig. 3c shows that the following dissociation reaction takes place: $1/2[\bar{1}\,\bar{1}\,0] = 1/6[\bar{1}\,\bar{2}\,1] + 1/6[\bar{2}\,\bar{1}\,1]$. This reaction has been analyzed for UO_2 by Fossati et al. (2013), and it was shown to be energetically favorable (at least for Morelon potential). However, Skelton and Walker (2017) mentions that due to the extremely narrow core of $1/2\langle 1\,1\,0\rangle\{1\,1\,0\}$, dissociation is unlikely to take place. Because splitting of the dislocation core happens on the $\{1\,1\,1\}$ atomic planes, the analysis conducted by Skelton and Walker (2017) using the Peierls-Nabarro model seems to be invalidated for this dislocation type. As shown by Fossati et al. (2013) for the Morelon potential, the maximum spacing (i.e., widening of the dislocation core) between the $1/6\langle 1\,1\,2\rangle$ partials is $d_p \approx 2b$. Roughly the same size of the stacking faults are seen in current simulation. Because these partials belong to the $\{1\,1\,1\}$ planes, in order for the dislocation line to move on the $\{1\,1\,0\}$ plane, they must recombine.

- *Emission of Frank loops* (Fig. 3d). At very high stresses, unpinning results in the emission of either $1/3[1\,1\,1]$ or $1/3[1\,1\,\bar{1}]$ Frank loops next to the pinning points. These loops are considerably more stable than the Shockley partials and are sessile. Hence, they have a detrimental effect on dislocation mobility. Interestingly, if a Frank loop forms next to two Shockley partials, they become connected by a $1/6\langle 1\,1\,0\rangle$ stair-rod dislocation. It was observed that by increasing the L_x dimension of the simulation cell from $24a$ to $48a$, which effectively increased the length of a dislocation line in simulation, also facilitates the formation of Frank loops.

To summarize the observations above, a map has been drawn to show the distinct regions in which a $1/2\langle 1\,1\,0\rangle$ screw dislocation moves according to different mechanisms (Fig. 4). This map also shows the nucleation rate of Shockley partials which has been evaluated by counting the total amount of extended segments of a screw dislocation split into two Shockley partials over a period of simulation time and divided by the length of the screw dislocation $l = L_x$. It can be seen that even in the simplest case when the dislocation does not

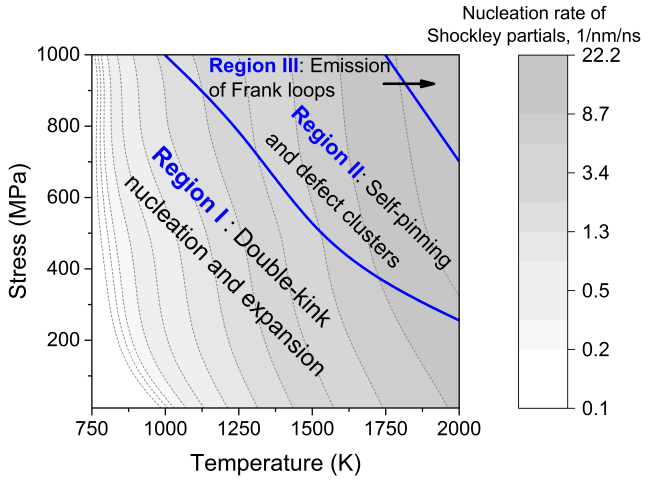

Figure 4: Stress-temperature map of motion constructed based on DXA analysis of the dynamics of $1/2\langle 1\,1\,0\rangle\{1\,1\,0\}$ screw dislocation lines in UO_2 from simulation

experience any self-pinning or formation of Frank partials and defect clusters, there is still a significant probability of forming Shockley partials on particular segments of the dislocation line during simulation runs.

3.3. Glide velocity data and interpretation of results

The dislocation velocity data extracted from MD simulations at different temperatures is shown on Fig. 5. Because the motion of $1/2\langle 1\,1\,0\rangle\{1\,1\,0\}$ screw dislocations is complex and involves many sub-processes and features as discussed in Sect. 3.2, there is no simple functional form that can describe all data obtained in this work. However, the collected data shows noteworthy trends:

- The velocity of the $1/2[1\,1\,0](1\,1\,0)$ screw dislocation at the highest temperature $T = 2000$ K and in a range of shear stresses σ is lower than for the $1/2[1\,1\,0](0\,0\,1)$ edge dislocation at the same conditions (Lunev et al., 2017a). On the other hand, at low temperatures ($T = 750 - 1250$ K), dislocation velocities are higher for screw dislocations. This is surprising considering the data on Peierls barriers recently reported by Skelton and Walker (2017). Although the motion of screw dislocation is thermally ac-

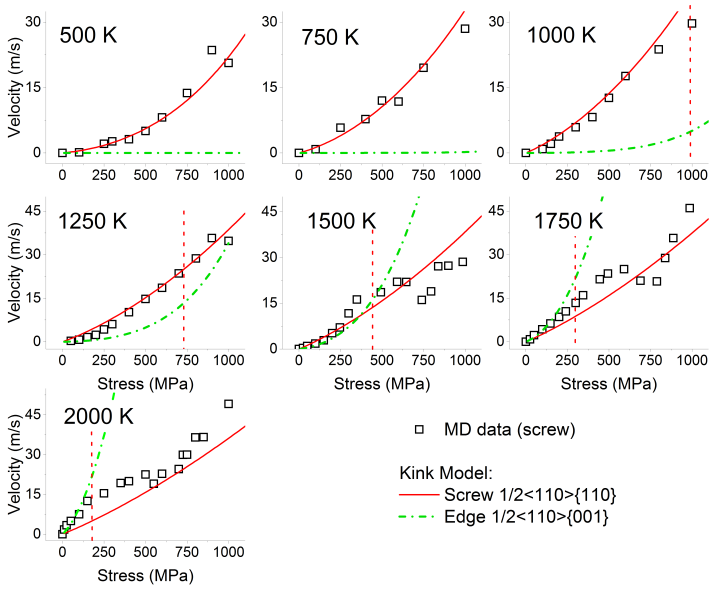

Figure 5: Glide velocity of the $1/2\langle 1\,1\,0\rangle\{1\,1\,0\}$ screw dislocation in UO_2 calculated at T = 500–2000 K and σ = 10–1000 MPa. Dotted vertical lines represent the critical stress at which self-pinning of dislocation segments happens and thus marks the applicability limit of the kink model. The red solid line is plotted using dislocation velocity expression with parameters from Table 1. Green dash-dotted line corresponds to the same expression, but with a different set of parameters previously obtained for the $1/2\langle 1\,1\,0\rangle\{0\,0\,1\}$ edge dislocation (Lunev et al., 2017a).

Table 1: Fitting parameters for the dislocation velocity expression based on the generalized double-kink nucleation and expansion formalism (Ref. [a])

Fitting parameter		Dislocation type and slip plane	
		Screw $\{1\,1\,0\}$	Edge $\{1\,0\,0\}$ [b]
A	($\mathrm{nm}^{3.25}$ / $\mathrm{eV}^{1/4}$ ns)	7.02 ± 0.39	$(0.74 \pm 0.33) \times 10^3$
B	($\mathrm{eV}^{1/2}\mathrm{nm}^{3/2}$)	0.096 ± 0.1	0.39 ± 0.03
U_0	(eV)	0.208 ± 0.013	1.38 ± 0.07

[a] Eq. (5) from Ref. [b]

[b] Lunev et al. (2017a)

tivated (as discussed in Sect. 3.2), the temperature dependence of glide velocity seems to be much weaker than in case of edge dislocations;

- At low stresses ($\sigma = 10$–300 MPa) and 750 K $\leq T \leq$ 1250 K, glide velocity increases slightly when the temperature decreases. This can probably be explained by the increased probability of splitting the dislocation segments into partials at higher temperatures (Fig. 4), and the delays in motion might be caused by finite time required for recombination;

- At $T = 1500$–2000 K two inflection points, one at moderate stress and one at high stress, are observed on the velocity-stress curve. The first one results in a slower rate at which dislocation velocity increases with stress. This may be attributed to the activation of self-pinning, as discussed in Sect. 3.2. The second one might be attributed to the activation of a more effective unpinning mechanism (formation of Frank loops).

Finally, the velocity function for the generalized double-kink nucleation and expansion model has been used to fit molecular dynamics data for the region where formation of double kinks was directly observed (this region is shown on Fig. 4). Fitting parameters for the velocity function of $1/2\langle 1\,1\,0\rangle\{1\,1\,0\}$ screw dislocation are summarized in Table 1. Using the latter, velocity-stress curves have been plotted at $T = 500$–2000 K on Fig. 5. To show how the velocity of screw ($1/2\langle 1\,1\,0\rangle\{1\,1\,0\}$) and edge ($1/2\langle 1\,1\,0\rangle\{0\,0\,1\}$) dislocations compare, curves for the velocity of edge dislocations produced with the same analytical model have also been plotted on the same graphs (Fig. 5). The screw dislocation from this work is much faster than the $1/2\langle 1\,1\,0\rangle\{0\,0\,1\}$ edge one (at temperature $T \leq 1000$ K), even though the latter supposedly corresponds to the primary slip system at high temperatures. This suggests there can be an exchange of weak and strong slip systems in UO_2 at $T < 1000$ K.

The kink model seems to offer a good approximation of the MD data at $T \leq$ 1250 K. However, the value of U_0 (effective Peierls barrier) presented in Table 1 is surprisingly low. At high temperatures ($T \geq 1500$ K), the model seems to

underestimate the actual velocity obtained with MD simulation. This could have the same reasons as discussed previously in (Lunev et al., 2017a), namely, breakdown of the elastic theory used for calculating the double-kink formation rate and inapplicability of the diffusion equation.

4. Conclusions

Thermally-activated motion of the $1/2\langle 1\,1\,0\rangle\{1\,1\,0\}$ screw dislocations was found to be composed of several processes, which are activated independently at different shear stress and temperature conditions. Nucleation and expansion of double kinks is still the main mechanism of motion under applied shear stress in most cases. However, even at low temperatures and stresses, the dislocation core experiences local splitting into partials, which are very unstable and tend to recombine rapidly. In other cases, the dislocations can generate pinning points randomly causing stuck segments and bending of the dislocation line across several Peierls valleys. At high stresses, the moving dislocation can eject Frank loops, which are sessile, and create other debris, such as clusters of point defects.

Surprisingly, the mobility of dislocations considered in this work is higher at $T \leq 1250$ K than the mobility of $1/2\langle 1\,1\,0\rangle\{0\,0\,1\}$ edge dislocations. The difference in velocity can reach several orders of magnitude at low temperatures. The latter is unexpected because $1/2\langle 1\,1\,0\rangle\{1\,1\,0\}$ were thought to have the highest high Peierls barrier (based, however, on a Peierls-Nabarro model which assumes planar dislocation core). This contradiction seems to support our original hypothesis that thermally-activated glide is not governed uniquely by the value of Peierls barrier defined at $T = 0$ K for a perfectly straight and non-dissociated dislocation.

Unfortunately, it is not yet possible to analytically describe the motion of screw dislocations in the full range of temperatures and stresses considered here. However, where kink formation has been observed, it was possible to use the generalized kink formalism and fit the model parameters to MD data. Presented results show good quality of fit and can be used for further meso-scale

calculations.

We hope that in future it will be possible to examine how charge transfer affects the mobility of screw dislocations, but this will require a well-developed many-body variable charge potential, which is yet to appear.

Acknowledgements

A.V.L. acknowledges the financial support of the Russian Foundation for Basic Research (personal grant No. 16-38-60016 mol_a_dk). Calculations were performed on Lomonosov supercomputer at the Supercomputing Centre of Moscow State University and on MVS-10P cluster at the Interdepartmental Supercomputing Centre of the Russian Academy of Sciences. A.V.L. would like to thank Dr. Teymur Aliev, head of laboratory at SSC RF TRINITI, and Dr. Abed Breidi, staff scientist at UKAEA, for extensive and fruitful discussion of simulation results.

References

Alamo, A., Lefèbvre, J.M., Soullard, J., 1978. Deformation plastique du bioxyde d'uranium: Observation des sous-structures de dislocations. Journal of Nuclear Materials 75, 145–153. doi:10.1016/0022-3115(78)90038-7.

Canon, R.F., Roberts, J.T.A., Beals, R.J., 1971. Deformation of UO_2 at high temperatures. Journal of the American Ceramic Society 54, 105–112.

Chartier, A., Onofri, C., Brutzel, L.V., Sabathier, C., Dorosh, O., Jagielski, J., 2016. Early stages of irradiation induced dislocations in urania. Applied Physics Letters 109, 181902. URL: https://doi.org/10.1063/1.4967191, doi:10.1063/1.4967191, arXiv:https://doi.org/10.1063/1.4967191.

Evans, A., Davidge, R., 1969. The strength and fracture of stoichiometric polycrystalline uo2. Journal of Nuclear Materials 33, 249 – 260. URL: http://www.sciencedirect.com/science/article/pii/0022311569900191, doi:https://doi.org/10.1016/0022-3115(69)90019-1.

Fossati, P., Brutzel, L.V., Devincre, B., 2013. Molecular dynamics simulation of dislocations in uranium dioxide. Journal of Nuclear Materials 443, 359–365.

Gilbert, M.R., Queyreau, S., Marian, J., 2011. Stress and temperature dependence of screw dislocation mobility in α-Fe by molecular dynamics. Physical Review B 84, 174103.

Hirth, J.P., Lothe, J., 1982. Theory of Dislocations. Krieger Publishing Company. URL: https://books.google.ru/books?id=LFZGAAAAYAAJ.

Kazantsev, A., Pokrovskii, V., 1970. Mobility of dislocations in a lattice with large peierls barriers. Soviet Journal of Experimental and Theoretical Physics 31, 362.

Keller, R.J., Mitchell, T.E., Heuer, A.H., 1988a. Plastic deformation in nonstoichiometric UO_{2+x} single crystals — II. deformation at high temperatures. Acta Metallurgica 36, 1073–1083.

Keller, R.J., Mitchell, T.E., Heuer, A.H., 1988b. Plastic deformation in nonstoichiometric UO_{2+x} single crystals —— I. deformation at low temperatures. Acta Metallurgica 36, 1061–1071.

Li, Y., Liang, T., Sinnott, S.B., Phillpot, S.R., 2013. A charge-optimized many-body potential for the u–uo 2 –o 2 system. Journal of Physics: Condensed Matter 25, 505401. URL: http://stacks.iop.org/0953-8984/25/i=50/a=505401.

Lunev, A., Kuksin, A., Starikov, S., 2017a. Glide mobility of the 1/2[1 1 0](0 0 1) edge dislocation in uo_2 from molecular dynamics simulation. International Journal of Plasticity 89, 85 – 95. URL: http://www.sciencedirect.com/science/article/pii/S0749641916302790, doi:https://doi.org/10.1016/j.ijplas.2016.11.004.

Lunev, A., Zazolin, A., Pchelyakov, D., Grigoriev, E., Isaenkova, M., Perlovich, Y., Krymskaya, O., 2017b. On morphological and microstructural changes in

uranium dioxide powder during binder-free hot pressing. Defect and Diffusion Forum 375, 114–122. doi:10.4028/www.scientific.net/DDF.375.114.

Marian, J., Cai, W., Bulatov, V.V., 2004. Dynamic transitions from smooth to rough to twinning in dislocation motion. Nature Materials 3, 158.

Morelon, N.D., Ghaleb, D., Delaye, J.M., Brutzel, L.V., 2003. A new empirical potential for simulating the formation of defects and their mobility in uranium dioxide. Philosophical Magazine 83, 1533–1555. doi:10.1080/1478643031000091454.

Murphy, S.T., Rushton, M.J., Grimes, R.W., 2014. A comparison of empirical potential models for the simulation of dislocations in uranium dioxide. Progress in Nuclear Energy 72, 27 – 32. doi:http://dx.doi.org/10.1016/j.pnucene.2013.09.010. symposium E @ E-MRS 2013 SPRING MEETING Scientific basis of the nuclear fuel cycle.

Parfitt, D.C., Bishop, C.L., Wenman, M.R., Grimes, R.W., 2010. Strain fields and line energies of dislocations in uranium dioxide. Journal of Physics: Condensed Matter 22, 175004.

Plimpton, S., 1995. Fast parallel algorithms for short-range molecular dynamics. Journal of Computational Physics 117, 1 – 19. URL: http://lammps.sandia.gov/, doi:10.1006/jcph.1995.1039.

Potashnikov, S.I., Boyarchenkov, A.S., Nekrasov, K.A., Kupryazhkin, A.Y., 2011. High-precision molecular dynamics simulation of UO_2–PuO_2: Pair potentials comparison in UO_2. Journal of Nuclear Materials 419, 217 – 225. doi:10.1016/j.jnucmat.2011.08.033.

Sattonnay, G., Tétot, R., 2013. Bulk, surface and point defect properties in uo 2 from a tight-binding variable-charge model. Journal of Physics: Condensed Matter 25, 125403. URL: http://stacks.iop.org/0953-8984/25/i=12/a=125403.

Scott, R., Hall, A., Williams, J., 1959. The plastic deformation of uranium oxides above 800° c. Journal of Nuclear Materials 1, 39 – 48. doi:https://doi.org/10.1016/0022-3115(59)90009-1.

Skelton, R., Walker, A.M., 2017. Peierls-nabarro modeling of dislocations in uo2. Journal of Nuclear Materials 495, 202 – 210. URL: http://www.sciencedirect.com/science/article/pii/S0022311517306815, doi:https://doi.org/10.1016/j.jnucmat.2017.08.024.

Stukowski, A., 2010. Visualization and analysis of atomistic simulation data with OVITO –- the open visualization tool. Modelling and Simulation in Materials Science and Engineering 18, 015012. URL: http://ovito.org/.

Stukowski, A., Bulatov, V.V., Arsenlis, A., 2012. Automated identification and indexing of dislocations in crystal interfaces. Modelling and Simulation in Materials Science and Engineering 20, 085007.

Yakub, E., Ronchi, C., Staicu, D., 2009. Computer simulation of defects formation and equilibrium in non-stoichiometric uranium dioxide. Journal of Nuclear Materials 389, 119 – 126. doi:10.1016/j.jnucmat.2009.01.029.

Yust, C., McHargue, C., 1969. Dislocation substructures in deformed uranium dioxide single crystals. Journal of Nuclear Materials 31, 121 – 137. URL: http://www.sciencedirect.com/science/article/pii/0022311569901871, doi:https://doi.org/10.1016/0022-3115(69)90187-1.